

Hydrogen Compatibility of Polymers for Fuel Cell Vehicles

Svenja Morsbach,* Dominik Giersch, Kai A. I. Zhang, Annett Schüßling, Dirk Weberskirch, and Alexander Börger*

So far, hydrogen compatibility of polymer materials was investigated, focusing on gaining insight in general degradation mechanisms. However, this is not yet sufficient for purposes of safety and performance requirements, for example, in the automotive industry and especially, the corresponding advanced material development, which needs meaningful and comprehensive data for prospective long time intervals. Therefore, herein, the applicability of forced aging regimes and the suitability of different analytical techniques for clarification of the underlying mechanisms are focused on. The study analyzes the behavior of polyether ether ketone, (thermoplastic) polyurethane and fluoroelastomer materials after prolonged aging in hydrogen atmosphere under pressure as it occurs in hydrogen fuel-cell vehicles. Material changes are investigated by electron microscopy, thermogravimetry, differential scanning calorimetry, and gas sorption measurements. Especially thermogravimetry turns out to indicate subtle material changes that are important indications for material choice.

from Germany, Japan, and United States of America on how to manage the development process for a Global Technical Regulation (GTR) on hydrogen-powered vehicles. It was decided to divide the development into two phases.

Phase 1 (GTR for hydrogen-powered vehicles), which was started in 2007, aimed to establish a GTR for hydrogen-powered vehicles based on a component level, subsystems, and whole vehicle crash test approach. For the crash testing, the GTR would specify that each contracting party will use its existing national crash tests but develop and agree on maximum allowable level of hydrogen leakage. Existing regulations and any available research and test data were to be used as a basis for the development of the first phase.

Phase 2 (assess future technologies and harmonize crash tests), initiated in 2017, was intended to amend the GTR to maintain its relevance with new findings based on new research and the state of the technology beyond 2010. Especially, one of the aims was to discuss how to harmonize crash test requirements for hydrogen and fuel cell vehicles regarding whole vehicle crash testing for fuel system integrity.^[1]

Already within Phase 1, material compatibility was subject to extensive discussions. However, in absence of a consensus, decisions were deferred to Phase 2. By then, standards and process recommendations had established methods for evaluating material compatibility of polymers in hydrogen applications such as American National Standards Institute/Canadian Standards Association Compressed Hydrogen Materials Certification 2 (ANSI/CSA CHMC 2).^[2] However, the test results used as a basis for these methods were achieved by only few research laboratories, mainly based in the industry, throughout the world. Therefore, the question on reproducibility, significance, and method improvement remained to be examined.

So far, hydrogen compatibility of polymer materials was investigated by different groups, whose results are summarized in a recent review by Balasooriya et al.^[3] However, this literature review makes clear that the information gained thus far is not yet sufficient. While some studies have concentrated on the degradation of polymers in hydrogen with respect to corresponding mass/volume changes,^[4] others have looked for structural and mechanical parameter changes including the analysis of relevant tensile^[5] or fracture properties^[6] or the changes of polymers under static high-pressure hydrogen conditions, later including also studies under repeated cycling.^[7] Recently, hydrogen

1. Introduction

In the context of an evolving hydrogen technology, in June 2005, the administrative committee 3 (AC.3) of United Nations Economic Council for Europe (UNECE) agreed to a proposal


S. Morsbach, K. A. I. Zhang
Department of Physical Chemistry of Polymers
Max Planck Institute for Polymer Research
55128 Mainz, Germany
E-mail: morsbachs@mpip-mainz.mpg.de

D. Giersch
Robert Bosch GmbH
70049 Stuttgart, Germany

A. Schüßling
Daimler Truck AG
70372 Stuttgart, Germany

D. Weberskirch
MAN Truck & Bus SE
90441 Nürnberg, Germany

A. Börger
Volkswagen AG
38440 Wolfsburg, Germany
E-mail: alexander.boerger@volkswagen.de

 The ORCID identification number(s) for the author(s) of this article can be found under <https://doi.org/10.1002/ente.202200018>.

© 2022 The Authors. Energy Technology published by Wiley-VCH GmbH. This is an open access article under the terms of the Creative Commons Attribution License, which permits use, distribution and reproduction in any medium, provided the original work is properly cited.

DOI: 10.1002/ente.202200018

compatibility of materials was investigated using microscopy and spectroscopic techniques.^[8] However, the study focused on nitrile-butadiene rubber (NBR) only. NBR was additionally part of other studies previously, mainly focusing on one or two specific material properties each.^[9] Sun et al. investigated hydrogen permeability of polyamide 6 as polymer liner material.^[10] With regard to sealing performance, theoretical studies were performed by Zhou et al., applying finite-element analysis to rubber O- and D-rings.^[11] In addition, some articles are limited on the importance of impurities^[12] or the general state of the art of polymer fuel cells.^[13] In summary, most of the conducted studies concentrate on very specific materials and/or characterization methodologies.

A fast and satisfactory material qualification for new materials to be used in hydrogen fuel-cell vehicle applications requires standardized and meaningful techniques as well as information about their applicability for material safety evaluation and regulation. Information on how long polymer materials can safely be applied in fuel cells and how this can be evaluated is obviously scarce. In particular, testing methods of materials that are in constant or at least regular contact with hydrogen, that is, tank, piping and receptacle, are needed. Therefore, it is the objective of this study to provide further experimental evidence for the hydrogen compatibility of polymeric materials and well-elaborated analytical procedures for additional tests, also suitable for samples taken from real vehicle applications. In this study we use a combination of microscopy, thermal analysis, and hydrogen adsorption measurements in order to determine the most useful analytical tools and provide general insight into the degradation mechanisms. As a result, we provide significant insight and fundamental knowledge to be used in the further regulatory and methodological development not only for the safety of hydrogen vehicles but also for other hydrogen applications and a methodology to scrutinize further materials.

2. Results

For the evaluation of material aging effects after hydrogen contact, several typical polymer materials to be applied in fuel cells, but not related to a specific type of fuel cell vehicle, were identified in this study and analyzed before and after hydrogen ageing treatment (as shown in Figure 1). These materials include

1) thermoplastic polyurethane (TPU)-shouldered test bars to be applied as sealing material, 2) polyether ether ketone (PEEK)-shouldered test bars as a potential material for polymer liners, 3) two different kinds of polyurethane (PU) O-rings for sealing, and 4) fluoroelastomer (FKM) O-rings for sealing.

For the treatment with hydrogen, currently there are no test standards so that the conditions were chosen according to professional and academic experience. The first aim was to accelerate possible aging effects using elevated temperature to detect occurring alterations within experimentally reasonable timeframes, which in this case meant incubation times not longer than 2–3 weeks (335 h). Accordingly, a temperature of 80 °C was selected to accelerate phenomena that would occur at 30 °C by a factor of 32 according to the Arrhenius law, while ensuring to stay within a temperature regime below the onset of thermal degradation (see also below in the section of thermal analysis). In addition, the aim was to approximate field conditions during fuel-cell application regarding the applied pressure. Typically, conventional fuel cell tanks are operated with a varying pressure of >100 bar. Therefore, the highest pressure that was reachable with our experimental infrastructure (85 bar) was used for the experiments. Thus, in summary, samples were incubated in H₂ atmosphere at 80 °C and 85 bar for 335 h (≈2 weeks).

All samples were subjected to several characterization techniques before and after H₂ incubation treatment. To evaluate different aspects of possible changes, the sample morphology, thermal properties, and H₂ adsorption were determined.

For morphological characterization of the samples before and after hydrogen incubation, scanning electron microscopy (SEM) imaging was conducted on all samples in two different ways. First, the surface of each sample (i.e., the hydrogen contact area) was imaged. Second, the freeze fracture surface of all samples was inspected by SEM. For this, samples were cooled in liquid nitrogen and subsequently mechanically broken. Then, the fracture surface was inspected.

Figure 2 shows the surfaces of TPU and PEEK samples before and after hydrogen incubation. Before hydrogen treatment, the surface of TPU was relatively smooth with minor roughness in the lower-micrometer range. After hydrogen incubation, the roughness of the surface increased significantly, indicating a substantial reaction to the incubation conditions. In principle, this could either be a result of material compression due to

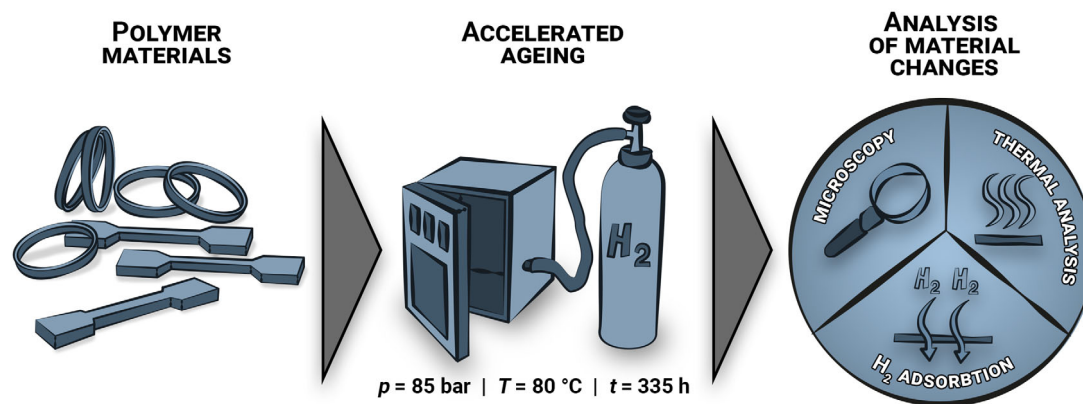


Figure 1. Schematic overview about performed experiments and study design.

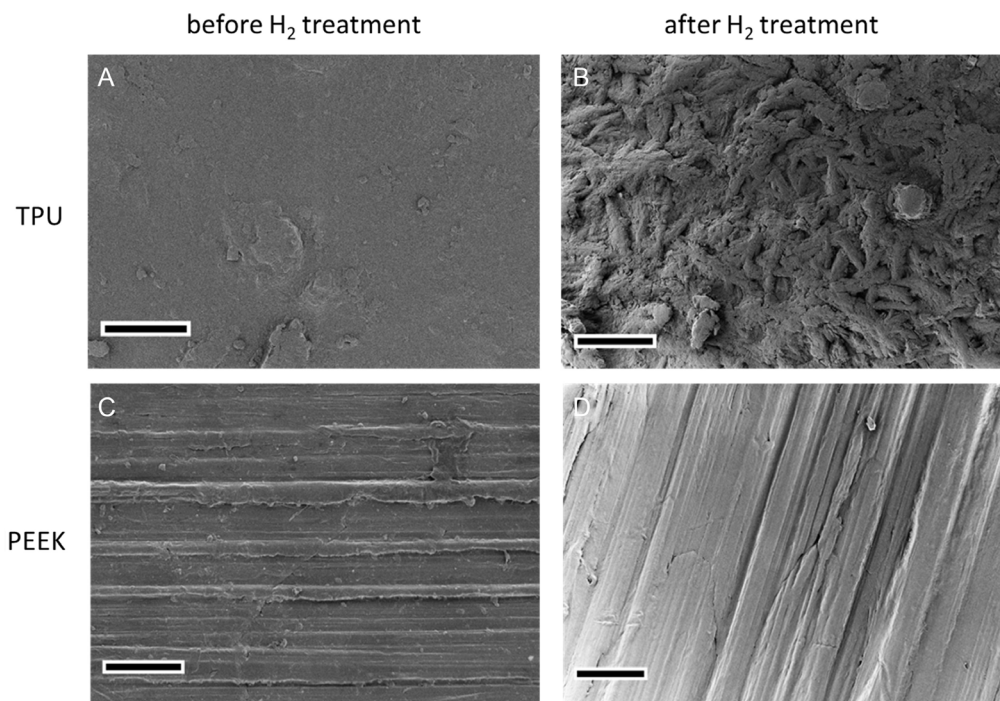


Figure 2. SEM images of the sample surface of A,B) TPU and C,D) PEEK samples before and after hydrogen incubation. Scale bar refers to 20 μm .

the high pressure or material that was “washed out” from in between the micrometer-sized particles. However, it seems unlikely that under hydrogen atmosphere PU material would be washed out. Rather, this could potentially be attributed to the different hardness of the PU segments, meaning that softer segments in the material might be compressed to a higher degree than the hard segments. In this case, the recorded effect might not be specific to hydrogen incubation but also occur in other atmospheres.

For the PEEK sample, irregular creasing can be detected before and after hydrogen incubation probably stemming from the sample manufacturing process. After hydrogen treatment, in some areas cracks were found on the material surface. In all cases, the edges of the cracks were rather smooth. This might suggest, that the cracks were already present in the material before the hydrogen incubation and were a result of the manufacturing process. For the application in fuel cells, however, it is critical that, ultimately, no defects occur in the final material.

For the analyzed O-rings (PU 1 + 2 and FKM), SEM images of the sample surfaces are shown in the supporting information (Figure S1 and S2, Supporting Information). Both PU samples showed regular indentations (spacing of roughly 150 μm) from the manufacturing of the O-rings. Apart from this, the material surface appeared very smooth and did not change before and after the hydrogen treatment. For FKM, the surface of the material shows roughness on the nanometer scale in all cases (before and after hydrogen treatment), indicating the presence of a high amount of inorganic particles. The hydrogen treatment did not result in any significant changes of the material surface.

In **Figure 3**, images of the freeze fracture surfaces of PU O-rings are shown as for these materials aging effects could be observed. Before hydrogen incubation, seemingly crystalline domains spanning several tens of micrometers could be found throughout both samples containing small nanometer-sized particles probably acting as seed crystals. After hydrogen incubation, these crystalline domains could not be distinguished anymore. However, the identified particles were still visible. This suggests that a physical rearrangement of the polymers might have occurred throughout the whole material, while the surface roughness of the sample was unaffected as described above. The material present in both PU samples behaved in a very similar way, meaning that also the overall chemical composition probably did not differ significantly.

Images of the freeze fracture surface of TPU are shown in Figure S3, Supporting Information. Both, before and after the hydrogen incubation, small pores were visible throughout the material, which might be a result of the manufacturing process. The general appearance of the material did not change after hydrogen treatment, indicating an overall effect only on the sample surface. In Figure S4, Supporting Information, freeze fracture surfaces of PEEK are shown before and after hydrogen incubation. The material shows a roughness on the nanometer scale, but no significant aging effects were found. This also suggests that any changes potentially resulting from hydrogen contact might only concern the sample surface. For FKM, a similar behavior was observed. Figure S5, Supporting Information displays the images taken from the freeze fracture surfaces of FKM O-rings. Also in the fracture surfaces, the high amount of inorganic particles was seen. However, again no significant effect of the hydrogen treatment could be detected.

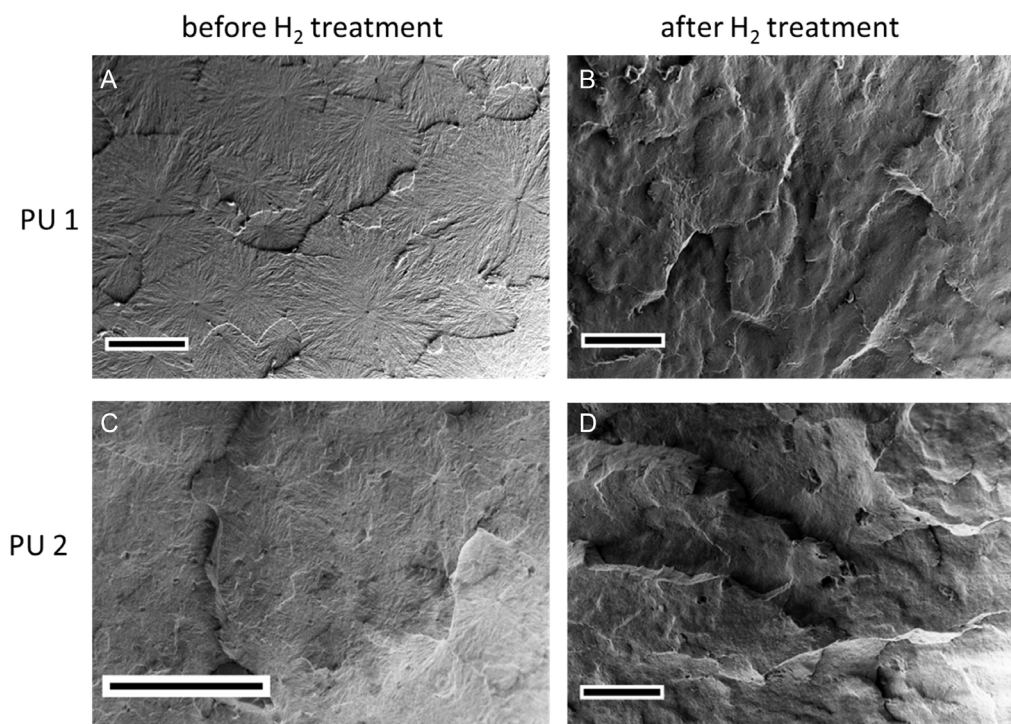


Figure 3. SEM images of the freeze fracture surface of A,B) PU 1 and C,D) PU 2 before and after hydrogen incubation. Scale bar refers to 20 μm .

Next, the obtained materials were subjected to thermal characterization. Thermal characterization methods give important hints about the properties of a polymer material and allow conclusions about its structure. Accordingly, in thermogravimetric analysis (TGA), the decomposition temperatures and associated mass loss of polymers can be determined in different gas atmospheres. Like this, information about the occurring decomposition reactions and with that the properties of the primary material can be obtained. In addition, thermal conversions can be detected with differential scanning calorimetry (DSC), including melting points and glass transition temperatures. These characteristic material properties depend highly on the chemical structure and crystallinity in the sample, which is possibly influenced by aging processes.

Thus, each sample was first subjected to TGA and subsequently DSC analysis as described in the Experimental Section. The obtained TGA results in N_2 and synthetic air for all samples before and after H_2 incubation are displayed in Table 1. Corresponding thermograms are shown in Figure S6–S10, Supporting Information.

For all samples, the temperatures of recorded decomposition steps were determined along with the corresponding mass loss. Interestingly, for each sample, significant changes of decomposition were visible, either during heating in N_2 or air atmosphere. More specifically, TPU and PU samples showed a rather similar decomposition behavior in N_2 . All three samples exhibit two distinct decomposition steps, where the first step occurs between ≈ 330 and ≈ 360 $^\circ\text{C}$ and the second step between ≈ 380 and ≈ 430 $^\circ\text{C}$. These decomposition steps are usually related to the hard and soft segments of polyurethane, respectively. The hard

segment is usually composed of the diisocyanate component, which can be aromatic or aliphatic. The soft segment is more variable and contains the diol component, which is mostly introduced as a polyol (polyether or polyester depending on application) and can vary in chain length. The decomposition processes occurring are accordingly influenced by the ratio and chemical structure of hard and soft segments as well as the type of polyol used. During thermal degradation, the urethane bond can degrade in various ways involving for example the dissociation into isocyanate and alcohol or the elimination of CO_2 yielding a primary or secondary amine. In literature, degradation ranges from ≈ 300 to ≈ 450 $^\circ\text{C}$ are reported in N_2 , where degradation temperatures increase with increasing fraction of hard segments.^[14] According to literature, the first step corresponds mainly to the liberation of CO_2 , while in the second step H_2O , HCN , and other small molecules might be released. In synthetic air, a degradation step between 500 and 600 $^\circ\text{C}$ was reported previously, which is also in line with the here-obtained results.^[14a] This step presumably corresponds to further decomposition of the previously formed char in the presence of oxygen. The TPU and PU samples all showed degradation in this temperature range with more or less pronounced steps in between. Importantly, H_2 incubation resulted in changed decomposition patterns, which were specific for each sample.

For TPU, only one degradation step was observed under N_2 , which could indicate that the two previous decomposition processes took place at similar temperature due to a changed nature of the segments or that the type of decomposition reaction has changed. Both scenarios include the precondition that changes throughout the material occurred. In addition, a new degradation

Table 1. Detected decomposition steps and associated mass loss of samples before and after hydrogen aging treatment determined by TGA. Detected changes are highlighted in bold.

sample		N ₂			Air			
		T ₁ [assoc. mass loss]	T ₂ [assoc. mass loss]	T ₃ [assoc. mass loss]	T ₁ [assoc. mass loss]	T ₂ [assoc. mass loss]	T ₃ [assoc. mass loss]	T ₄ [assoc. mass loss]
TPU	−H ₂	339 °C [19%]	388 °C [71%]	–	339 °C [77%]	549 °C [16%]	–	–
	+ H ₂	368 °C [88%]	622 °C [8%]	–	336 °C [78%]	547 °C [17%]	–	–
PEEK	−H ₂	592 °C [35%]	650 °C [16%]	–	589 °C [31%]	653 °C [63%]	–	–
	+ H ₂	592 °C [39%]	727 °C [4%]	–	589 °C [31%]	659 °C [62%]	–	–
PU 1	−H ₂	348 °C [40%]	425 °C [52%]	–	347 °C [31%]	428 °C [30%]	448 °C [10%]	555 °C [25%]
	+ H ₂	353 °C [15%]	421 °C [55%]	–	341 °C [32%]	427 °C [31%]	449 °C [8%]	559 °C [21%]
PU 2	−H ₂	356 °C [28%]	406 °C [64%]	–	360 °C [31%]	405 °C [42%]	544 °C [23%]	–
	+ H ₂	355 °C [26%]	400 °C [65%]	–	348 °C [37%]	415 °C [36%]	569 °C [16%]	–
FKM	−H ₂	434 °C [8%]	491 °C [44%]	561 °C [4%]	440 °C [5%]	492 °C [48%]	588 °C [37%]	–
	+ H ₂	434 °C [6%]	490 °C [45%]	561 °C [5%]	425 °C [7%]	491 °C [47%]	544 °C [4%]	630 °C [34%]

step at even higher temperatures occurred (>600 °C), leading to an overall higher mass loss (96%) versus the thermal degradation before H₂ treatment (90%).

For PU 1, changes due to hydrogen incubation are mainly visible in the measurements under N₂ atmosphere. Here, significantly less mass loss was found during the first decomposition step, leading to an overall mass loss of only 70% versus 92% before the hydrogen treatment. Interestingly, these measurements suggest a higher thermal stability of the material after hydrogen incubation.

In contrast, for PU 2, changes after hydrogen incubation were only recorded in synthetic air atmosphere. Decomposition steps two and three were shifted to slightly higher temperatures and step one to a lower temperature. Overall, the associated mass loss was lower, corresponding to a higher thermal stability of the material. These results suggest that for TPU/PU the decomposition profile and with that the reaction to the applied aging procedure highly depend on the nature of the respective polymer segments. Especially the ratio of hard-to-soft segments might be crucial as this also determines the compressibility of the material.

Similar to TPU/PU samples, PEEK in general showed two distinct decomposition steps independent from the different conditions. Under N₂ atmosphere, a significant amount of char formation was observed, meaning that roughly only 50% of mass loss was detected. This behavior corresponds to the observations reported in literature and is a result of the high degree of aromatic groups in the main polymer chain.^[15] The onset of decomposition generally occurred roughly from 575 °C on, indicating that the material is very stable up to high temperatures. As a dominant degradation mechanism during the first decomposition step, random chain scission of ether and ketone bonds were reported. Products of this step are mainly phenol, CO, and CO₂.^[16] At higher temperatures, under N₂, the formation of radical intermediates and further decomposition of these was reported. In air, the second decomposition step could be attributed to oxidation of the carbonaceous char formed in the first decomposition step. Comparing the materials before and after

H₂ treatment, the only significant change that was found corresponds to a higher stability of the material under N₂ in the second decomposition step. Here, less mass loss was detected at a higher decomposition temperature. The reason for this effect might be a partial reduction of ketone groups leading to a higher stability of the resulting polymer by additional hydrogen bonds and the healing of eventual point defects (free radicals, residual C=C double bonds etc.) by forming additional C—H bonds.

For the FKM material, three different decomposition steps were found in N₂ as well as under air atmosphere. The main step in N₂ was the second decomposition step, while in air the third step introduced another significant part of degradation reactions. In literature, usually one single decomposition step in N₂ was reported in the range of 430–500 °C, depending on the monomer composition.^[17] The occurring degradation processes are described to be very complex, but can generally be divided into two main routes: decomposition of chain carbon bonds (main) and decomposition by splitting off hydrogen and fluorine as HF (secondary).^[18] During thermal treatment, the oxidation of C—F bonds might take place in the presence of oxygen as described in literature.^[19] This could lead to the generation of carboxylic groups and subsequently further oxidation to CO₂. This process might correspond to the third main degradation step in synthetic air. Changes after hydrogen treatment were not found for the degradation in N₂, but for the decomposition in the high-temperature regime in air, indicating that the occurring oxidation reactions might have changed.

After evaluating the thermal decomposition processes before and after hydrogen aging treatment, phase transitions occurring in the materials were determined by DSC. All detected phase transitions during the second heating cycle are summarized in Table 2. The corresponding melting curves are shown in Figure S11–S15, Supporting Information.

For TPU samples, before and after aging, similar heating curves were obtained, showing one main phase transition corresponding to a glass transition point (*T_g*). A *T_g* below 0 °C can be attributed to the soft segment of the polymer, while potential

Table 2. Detected phase transitions in samples before and after hydrogen aging treatment determined by DSC.

Sample		T_g [°C]	Δc_p [J g ⁻¹ K ⁻¹]	T_m [°C]
TPU	-H ₂	-47	0.477	-
	+H ₂	-47	0.656	-
PEEK	-H ₂	-	-	339
	+H ₂	-	-	340
PU 1	-H ₂	-68	0.322	-
	+H ₂	-71	0.342	-
PU 2	-H ₂	-55	0.278	229
	+H ₂	-52	0.159	230
FKM	-H ₂	-54	0.148	-
	+H ₂	-54	0.080	-

glass transition temperatures of the hard segment should occur at much higher temperatures.^[14b] In addition, the change in heat capacity Δc_p was determined for the glass transition points. While the glass transition temperatures did not differ significantly, the associated heat capacity changes indicate a higher degree of crystallinity throughout the sample before the aging treatment. Without exact knowledge about the chemical composition it is, however, very hard to interpret the obtained changes. Finally, other significant phase transitions than the T_g at low temperatures could not be observed, suggesting a high crystallinity of the hard segment. Thus, we cannot conclude anything about changes occurring during H₂ treatment in the hard segment. In PEEK samples, one main phase transition corresponding to a melting point (T_m) was observed. The determined T_m before and after aging exactly matches the literature reported melting point of 339 °C measured with a heat rate of 10 K min⁻¹.^[20] Here, it can be concluded that the thermal properties of the material were not affected by the hydrogen incubation procedure.

For both PU 1 samples, as a main phase transition a glass transition point was detected, which is also in line with the T_g determined for TPU. In contrast to TPU, however, the change of heat capacity Δc_p did not yield any difference after the aging procedure. Several other minor phase transitions were detected in addition for both samples, probably resulting from additives in the material. In summary, within the accuracy of the measurement, no significant changes of the thermal properties were found. For PU 2 samples, again glass transition points were recorded, showing no significant differences after the aging procedure. The associated change of heat capacity Δc_p was determined to be lower after hydrogen incubation, presenting a significant difference regarding the sample crystallinity. However, from the morphological characterization, the opposite trend could have been expected (lower crystallinity after incubation). In addition, as another main phase transition, a melting point was recorded, which again did not change significantly.

Finally, also the thermal phase transitions occurring in FKM were determined via DSC, before and after hydrogen treatment. The main recorded phase transition was a glass transition point. The temperature did not change significantly related to the hydrogen incubation. The determination of change in heat

capacity Δc_p yielded a significant decrease after the aging treatment. In principle, this indicates again a higher degree of crystallinity in the sample after hydrogen incubation. In addition, after aging a small peak corresponding to a melting point became visible at around 0 °C. However, this peak was very small and, thus, probably not a result of the main polymer material. Other phase transitions occurring might be related to additives used in the O-rings, similar to PU 1 and 2.

In a last step, the general hydrogen adsorption capacity was determined via Brunauer–Emmet–Teller (BET) adsorption measurements for all samples. These measurements were performed on the samples without any pretreatment. The amount of adsorbed hydrogen per sample mass was monitored depending on the relative hydrogen pressure (see Figure 4). For each sample, the final amount of adsorbed hydrogen is summarized in Table 3 together with the sample surface area calculated according to the BET theory. The calculation is performed under the assumption that only physical interaction between hydrogen and the sample takes place. In these measurements it is not possible to precisely distinguish between physisorption and chemisorption, but under the given conditions and rather inert nature of the polymer materials, a chemical reaction between hydrogen and the sample material seems unlikely.

The determined amount of adsorbed hydrogen was relatively similar for four out of the five available materials. TPU, PU, and FKM samples all adsorbed hydrogen in a range of 0.004–0.012 mmol g⁻¹ corresponding to surface areas of 0.08–0.37 m² g⁻¹, which correspond to generally very low hydrogen adsorption. For PEEK, a higher amount of adsorbed hydrogen was recorded (0.124 mmol g⁻¹), which also resembles a higher available surface area (3.01 m² g⁻¹).

3. Discussion

For this study, five different sample types were selected, subjected to hydrogen aging treatment and subsequently characterized with different analytical methods. For the aging treatment, an elevated temperature of 80 °C was chosen after TGA of the

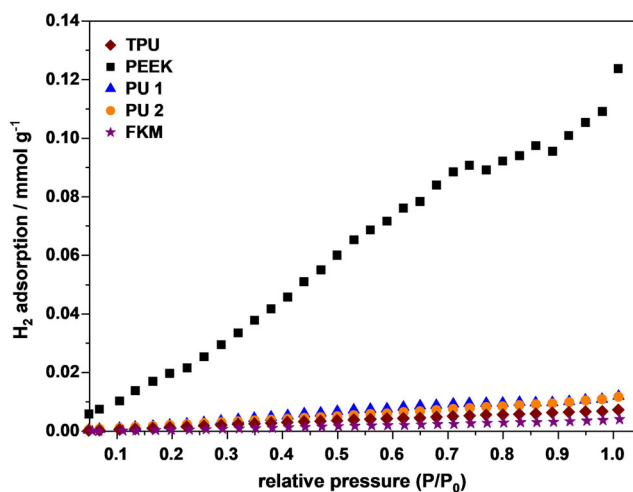


Figure 4. Hydrogen adsorption determined via BET for all samples without aging treatment. Measurements were performed at 298 K and 1 atm.

Table 3. Hydrogen adsorption and surface area determined via BET measurements.

Sample	H ₂ (adsorbed) [cm ³ g ⁻¹]	H ₂ (adsorbed) [mmol g ⁻¹]	BET surface area [m ² g ⁻¹]
TPU	0.161952	0.00723	0.1726
PEEK	2.771328	0.12372	3.0116
PU 1	0.266784	0.01191	0.3694
PU 2	0.261632	0.01168	0.2231
FKM	0.090496	0.00404	0.0847

untreated samples, which revealed that all samples were stable under these conditions. Subsequently, various analytical techniques were applied, showing that for all samples differences before and after hydrogen incubation could be detected. This indicates that the chosen treatment conditions (H₂ incubation at 80 °C, 85 bar, 335 h) were in principle suitable to induce aging processes in the selected materials.

The conducted SEM measurements indicate that sample imaging is a very useful tool to obtain insights about the morphological changes associated with hydrogen treatments. Ideally, it should be ensured that the same sample specimen is used for imaging before and after the incubation to rule out potential differences stemming from the manufacturing process. Electron microscopy (EM) provides a very detailed view on the samples so that it is ideal for fundamental research on different materials, but rather demanding in terms of resources (high equipment cost, personnel effort) so that a fast screening of a high sample number is not practical. Other microscopy methods might provide easier access to fast imaging, but it has to be clarified whether the accessible resolution is suitable to resolve the aging effects.

Thermal characterization yields valuable information regarding material properties before and after the conducted incubation processes. Occurring changes due to the treatment were mainly visible by TGA, which offers a rather fast and convenient way to detect already minor material differences. Further investigations are needed, however, to clarify the nature of these variations. The instrument cost is moderate and also required time and personnel resources are acceptable for sample screening.

DSC, on the other side, allows estimating the influence on material performance based on its physical appearance (mainly the glass transition point). In this study, changes were not detected in these measurements regarding the phase transition

temperatures, but the determination of change in heat capacity might present an opportunity for further evaluation. However, this is only possible if the chemical structure of the material is known exactly. In general, the method might be valuable as a quality control step regarding the application of the materials as glass transition points are decisive for material performance.

The amount of hydrogen interacting with a given material surface can be determined via BET measurements. In general, the absolute amount of adsorbed H₂ is low for all polymer materials. Differences between the materials can be identified, but definite interpretations of the ongoing interaction mechanisms are not possible as it cannot be precisely distinguished between chemi- and physisorption. It might be that hydrogen diffuses into the materials to a certain extent depending on the material properties (like micro- or nanoporosity). Otherwise, the gas can associate mainly on the sample surface. As the measurement times are rather short compared with the long-term aging treatments and no elevated pressure or temperature conditions were present, these interaction mechanisms seem to be favored. For the analysis of hydrogen compatibility in fuel-cell vehicles, BET measurements might be helpful to evaluate the sample surface areas available for interaction. The higher the available surface area, the higher is the potential for irreversible hydrogen aging effects. For the determination of hydrogen uptake (physical or chemical) under the chosen storage conditions (335 h, 80 °C, 85 bar), BET measurements are not suitable with the current equipment conditions.

Finally, the evaluation of all techniques applied in this study regarding the characterization of hydrogen aging effects is summarized in **Table 4**. From the here conducted analyses, we rate TGA as the most valuable characterization technique.

To further obtain insight about the processes occurring upon the material incubation, it needs to be clarified whether the detected effects are indeed a result of the contact to hydrogen. It is also possible that they are caused by the incubation conditions such as the elevated temperature and pressure. Therefore, future investigations should include reference samples that were incubated under the same conditions but in inert atmosphere, for example, nitrogen. Due to the limited number of sample specimen, this was not possible in the here conducted study.

Obtaining detailed information about changes in the chemical structure of the applied polymer materials remains to be more challenging than physicochemical analysis. In principle, for example, solid-state NMR (ssNMR) is able to resolve very detailed chemical information of the sample materials. However, the

Table 4. Overview about performed measurements, detected material changes after hydrogen treatment, and technique evaluation.

Method	Changes detected	Recommendation ^{a)}	Remarks
EM	Surface: TPU, (PEEK) Cross section: PU 1 + 2	++	High resource demand (cost, personnel), very high resolution, visual inspection of samples
TGA	All samples	+++	Highest detection rate of aging effects, relatively low resource demand
DSC	TPU, PU 1 + 2	+	Relatively low resource demand, requires more research effort to interpret effects
BET	N.D.	+	Conditions are not similar to aging treatment, moderate resource demand

^{a)}Scale from +++ (highly recommended) to + (recommended within limits)

resource demand is very high (high instrument cost, personnel, and time effort) and it is not a routine technique. Thus, the application of ssNMR for routine evaluation of aging effects is not recommended. As an alternative, IR spectroscopy might be suitable to analyze the chemical structure of polymers.

To assess the final material performance (e.g., sealing ability) when it comes to the application, we advise to include mechanical analysis of the sample specimen. As a significant number of sample specimen is required to obtain reliable statistics, this method might be applied at a later development stage, but its inclusion is strongly recommended regarding material safety evaluation. Further, it has to be kept in mind that the accelerated aging conditions used in this study are not exactly the same as the conditions for long-term aging of materials under field usage conditions. Thus, a direct correlation of the observed effects with events occurring on the road is only possible after examination of a high number of real fuel-cell vehicle samples of different designs and applications. However, using accelerated aging conditions enables fast prescreening of materials for potential safety issues and, thus, poses a significant benefit for the first step of fuel-cell design.

4. Conclusion

In summary, the conducted study presents an overview about possible testing procedures and their applicability for the development of standardization guidelines and yields information about effects occurring after accelerated hydrogen aging treatments. Five different polymer material samples (TPU/PU, PEEK, FKM) were investigated before and after hydrogen ageing treatments. Morphological changes of the materials, either on the material surface or within the materials, were found by applying SEM, which is a valuable tool for fundamental research about the ongoing processes. For all samples, aging effects could be detected via TGA, being the most sensitive method to resolve the occurring changes. Additionally, information about the phase transitions of the materials was obtained using DSC, which revealed only minor changes related to the heat capacity of the glass transition points. Last, hydrogen adsorption of the samples was evaluated by BET measurements, yielding information about the material surface area available for interaction (and, thus, for aging processes). The performed analyses provide highly useful information regarding the applicability of various characterization methods for hydrogen compatibility and might serve as a base for further standardization efforts. For the future, samples from real vehicle applications should be investigated with the analytical techniques developed in this study to maximize information about field relevance.

5. Experimental Section

Materials: TPU and PEEK were obtained from Robert Bosch GmbH. PU O-rings were obtained from Volkswagen AG. All material samples before and after aging were stored in the dark at a constant temperature of $T = 20\text{ }^{\circ}\text{C}$. For the aging treatment samples were incubated at $T = 80\text{ }^{\circ}\text{C}$ and $p = 85\text{ bar}$ for 335 h in H_2 atmosphere.

Scanning Electron Microscopy: Polymer samples were cut into $1\text{ cm} \times 1\text{ cm}$ pieces (shouldered test bars) or 1 cm-long O-ring cut-outs. For each sample, the native surface as well as a freeze fracture surface

was investigated. To produce fracture planes, 1 cm sample pieces were scratched on the surface, mounted to two holders, and subsequently immersed into liquid nitrogen. After the cooling down of the sample was completed (no bubbling observed anymore), the sample was cracked manually with a second holder along the scratchline. As an exception, PEEK samples were taken out of the nitrogen and cracked afterward to achieve better handling possibilities (samples required more force to be cracked). Morphological characterization of the polymer samples was then performed via low-voltage scanning electron microscopy (LV-SEM). Imaging was performed on a Leo 1530 Gemini Schottky FEG-SEM microscope with 0.1–1.0 kV landing voltage.

Differential Scanning Calorimetry: Samples were transferred into DSC sample aluminum pans (100 μL volume, Mettler-Toledo GmbH, Gießen, Germany) and covered with aluminum lids. DSC measurements were performed on a DSC 823 instrument (Mettler-Toledo GmbH, Gießen, Germany). Heating–cooling–heating cycles were recorded with a heating/cooling rate of 10 K min^{-1} between -140 and $+520\text{ }^{\circ}\text{C}$ for PEEK and -140 and $+280\text{ }^{\circ}\text{C}$ for all other samples. The measurements were performed under nitrogen atmosphere with a flow of 30 mL min^{-1} . For all samples, the second heating cycle was evaluated to avoid effects due to sample history.

Thermogravimetric Analysis: Samples were transferred into aluminum oxide sample pans (ME-24 124, 150 μL volume, Mettler-Toledo GmbH, Gießen, Germany). TGA measurements were performed on a TGA/DSC 3 instrument (Mettler-Toledo GmbH, Gießen, Germany). Heating curves were recorded with a heating rate of 10 K min^{-1} between RT and $900\text{ }^{\circ}\text{C}$ for all samples. The measurements were performed for all samples once under nitrogen and once under synthetic air atmosphere with a flow of 50 mL min^{-1} each. For all samples, the mass loss was normalized according to initial sample mass.

BET: The samples were degassed at $120\text{ }^{\circ}\text{C}$ for 6 h under vacuum. The H_2 adsorption behavior of the samples was measured on a 3Flex Adsorption Analyzer of Micromeritics at 298 K. The saturated pressure was 760 mm Hg (1 atmosphere) and the pressure change rate was $\approx 5\text{ mm Hg min}^{-1}$. The data were analyzed using the software MicroActive by Micromeritics. The BET surface area and H_2 adsorption were calculated via nonlocal density functional theory (NLDFT) models.

Supporting Information

Supporting Information is available from the Wiley Online Library or from the author.

Acknowledgements

The authors thank the Institute for Organic Chemistry of Clausthal University of Technology for performing hydrogen aging treatments. Additionally, we acknowledge Gunnar Glaßer for SEM imaging and Petra Räder for help with the thermal analysis. Furthermore, the authors are thankful to Zhuangfei Qian and Sizhe Li of the Department of Materials Science at Fudan University for performing the BET measurements. Funding was provided by the Forschungsvereinigung Automobiltechnik (FAT) e.V.

Open Access funding enabled and organized by Projekt DEAL.

Conflict of Interest

The authors declare no conflict of interest.

Data Availability Statement

The data that support the findings of this study are available from the corresponding author upon reasonable request.

Keywords

characterization, degradation, fuel cells, hydrogen, polymers

Received: January 7, 2022

Revised: June 9, 2022

Published online:

- [1] UNECE, Global Technical Regulations (GTRs) Transport, <https://unece.org/transport/standards/transport/vehicle-regulations-wp29/global-technical-regulations-gtrs>, (accessed: May, 2022).
- [2] ANSI/CSA CHMC 2: 2019-08-01, Test methods for evaluating material compatibility in compressed hydrogen applications - Polymers, **2019**, <https://www.csagroup.org/store/product/2427320/> (accessed: June, 2022).
- [3] W. Balasooriya, C. Clute, B. Schrittmesser, G. Pinter, *Polym. Rev.* **2021**, *1*, 175.
- [4] S. Castagnet, J.-C. Grandidier, M. Comyn, G. Benoît, *Int. J. Hydrogen Energy* **2010**, *35*, 7633.
- [5] S. Castagnet, J.-C. Grandidier, M. Comyn, G. Benoît, *Int. J. Press. Vessel. Pip.* **2012**, *89*, 203.
- [6] J. Yamabe, S. Nishimura, *Int. J. Hydrogen Energy* **2009**, *34*, 1977.
- [7] N. C. Menon, A. M. Krüzenga, K. J. Alvine, C. San Marchi, A. Nissen, K. Brooks, in *ASME 2016 Pressure Vessels and Piping Conf., Vol. Volume 6B: Materials and Fabrication*, Vancouver, Canada, **2016**.
- [8] K. L. Simmons, W. Kuang, S. D. Burton, B. W. Arey, Y. Shin, N. C. Menon, D. B. Smith, *Int. J. Hydrogen Energy* **2021**, *46*, 12300.
- [9] a) K. Ohyama, H. Fujiwara, S. Nishimura, *Int. J. Hydrogen Energy* **2018**, *43*, 1012; b) J. K. Jung, S. K. Jeon, K.-T. Kim, C. H. Lee, U. B. Baek, K. S. Chung, *Sci. Rep.* **2019**, *9*, 13035; c) H. Ono, H. Fujiwara, S. Nishimura, *Int. J. Hydrogen Energy* **2018**, *43*, 18392; d) H. Fujiwara, H. Ono, S. Nishimura, *Int. J. Hydrogen Energy* **2015**, *40*, 2025. e) S. Nishimura, H. Fujiwara, *Chem. Phys. Lett.* **2012**, *522*, 43.
- [10] Y. Sun, H. Lv, W. Zhou, C. Zhang, *Int. J. Hydrogen Energy* **2020**, *45*, 24980.
- [11] a) C. Zhou, J. Zheng, C. Gu, Y. Zhao, P. Liu, *Int. J. Hydrogen Energy* **2017**, *42*, 11996; b) C. Zhou, G. Chen, P. Liu, *J. Fail. Anal. Prev.* **2018**, *18*, 846.
- [12] Z. Du, C. Liu, J. Zhai, X. Guo, Y. Xiong, W. Su, G. He, *Catalysts* **2021**, *11*, 393.
- [13] Y. Wang, D. F. Ruiz Diaz, K. S. Chen, Z. Wang, X. C. Adroher, *Mater. Today* **2020**, *32*, 178.
- [14] a) M. Herrera, G. Matuschek, A. Kettrup, *Polym. Degrad. Stab.* **2002**, *78*, 323; b) M. Kannan, S. S. Bhagawan, S. Thomas, K. Joseph, *J. Therm. Anal. Calorim.* **2013**, *112*, 1231; c) A. K. Barick, D. K. Tripathy, *J. Appl. Polym. Sci.* **2010**, *117*, 639; d) A. Saiani, W. A. Daunch, H. Verbeke, J. W. Leenslag, J. S. Higgins, *Macromolecules* **2001**, *34*, 9059.
- [15] P. Patel, T. R. Hull, R. W. McCabe, D. Flath, J. Grasmeyer, M. Percy, *Polym. Degrad. Stab.* **2010**, *95*, 709.
- [16] a) L. H. Perng, C. J. Tsai, Y. C. Ling, *Polymer* **1999**, *40*, 7321; b) M. Day, J. D. Cooney, D. M. Wiles, *J. Anal. Appl. Pyrolysis* **1990**, *18*, 163.
- [17] a) A. Singh, P. K. Soni, M. Singh, A. Srivastava, *Thermochim. Acta* **2012**, *548*, 88; b) M. A. Kader, A. K. Bhowmick, *Polym. Degrad. Stab.* **2003**, *79*, 283.
- [18] I. Banik, A. K. Bhowmick, S. V. Raghavan, A. B. Majali, V. K. Tikku, *Polym. Degrad. Stab.* **1999**, *63*, 413.
- [19] H. Lee Jin, W. Bae Jong, C. Choi Myoung, Y.-M. Yoon, H. Park Sung, N.-J. Jo, *Elastomers Compos.* **2018**, *53*, 213.
- [20] M. C. Kuo, C. M. Tsai, J. C. Huang, M. Chen, *Mater. Chem. Phys.* **2005**, *90*, 185.